Effects of interactions on the relaxation processes in magnetic nanostructures

ATKINSON, Lewis J., OSTLER, Thomas <http://orcid.org/0000-0002-1328-1839>, HOVORKA, O., WANG, K. K., LU, B., JU, G. P., HOHLFELD, J., BERGMAN, B., KOOPMANS, B. and CHANTRELL, Roy W.

Effects of interactions on the relaxation processes in magnetic nanostructures

Lewis J. Atkinson,[1,*] Thomas A. Ostler,[2,†] O. Hovorka,[3] K. K. Wang,[4] B. Lu,[4] G. P. Ju,[4] J. Hohlfeld,[5] B. Bergman,[6] B. Koopmans,[6] and Roy W. Chantrell[1]

[1]*Department of Physics, University of York, Heslington, York YO105DD, United Kingdom*
[2]*Département de Physique, Universitè de Liége (B5), B-4000 Liége, Belgium*
[3]*Engineering and the Environment, University of Southampton, Southampton SO16 7QF, United Kingdom*
[4]*Seagate Technology, 47010 Kato Road, Fremont, California 94538, USA*
[5]*Seagate Technology, 7801 Computer Avenue, Bloomington, Minnesota 55435, USA*
[6]*Department of Applied Physics, Technische Universiteit Eindhoven, P.O. Box 513, 5600 MB Eindhoven, Netherlands*

(Received 13 May 2016; revised manuscript received 10 August 2016; published 28 October 2016)

Controlling the relaxation of magnetization in magnetic nanostructures is key to optimizing magnetic storage device performance. This relaxation is governed by both intrinsic and extrinsic relaxation mechanisms and with the latter strongly dependent on the interactions between the nanostructures. In the present work we investigate laser induced magnetization dynamics in a broadband optical resonance type experiment revealing the role of interactions between nanostructures on the relaxation processes of granular magnetic structures. The results are corroborated by constructing a temperature dependent numerical micromagnetic model of magnetization dynamics based on the Landau-Lifshitz-Bloch equation. The model predicts a strong dependence of damping on the key material properties of coupled granular nanostructures in good agreement with the experimental data. We show that the intergranular, magnetostatic and exchange interactions provide a large extrinsic contribution to the damping. Finally we show that the mechanism can be attributed to an increase in spin-wave degeneracy with the ferromagnetic resonance mode as revealed by semianalytical spin-wave calculations.

DOI: 10.1103/PhysRevB.94.134431

I. INTRODUCTION

Over the past few decades the demand for information storage has increased at unprecedented rates. This has driven forward huge advances in the areal density of hard disk drives (HDD) based on magnetic storage. These increases have led to hard drive (granular) media containing much smaller grains located in smaller areas. In an ideal scenario the ability to control the magnetic orientation of individual grains would be possible without the effects of interactions between them. However, in structured magnetic materials at the nanoscale this ideal can never be reached. In reality the nanostructures are coupled. This coupling can arise from a number of mechanisms: the long-ranged dipole-dipole field, direct exchange between grains through magnetic impurities across the interstitial region [1], or via superexchange via oxides in the interstitial boundary layer. The role of interactions in relaxation processes in magnetic materials has long been studied [2–6], though it is often very difficult to determine individual mechanisms by which the system relaxes.

The key measurable quantity that governs the relaxation of the magnetization is the effective damping. This parameter determines the dynamics of the magnetization after an external stimulus and, importantly for granular magnetic media, it governs the speed at which a bit can be reversed. A large value of damping is desirable to speed up the writing process and reduce transition noise in perpendicular magnetic recording (PMR) and to reduce the dc noise arising from backswitching during the heat assisted magnetic recording (HAMR) process. Although its effect on recording performance is significant, the origin of damping is poorly understood. Mo *et al.* [6] carried out a detailed analysis of FMR data on CoCrPt perpendicular media, concluding that the intrinsic damping from magnon-electron scattering was as low as 0.004, over an order of magnitude smaller than the values usually obtained for the total damping. Mo *et al.* ascribe the major contribution to the damping as arising from inhomogeneity line broadening and grain boundary two-magnon scattering. However, another extrinsic candidate contribution to damping arises from the effects of intergranular interactions. In the present work we investigate the effects of magnetostatic and exchange interactions on the effective damping of perpendicular media. It is shown that the interactions give rise to an increase in damping which is due to the presence of long-ranged dipole-dipole spin wave modes. The introduction of exchange interaction results in a stiffening of the magnetization and a consequent reduction in damping, demonstrated experimentally for a series of CoCrPt granular media, and verified by micromagnetic modeling. We furthermore use a simplified model of spin waves [2] to show that the interplay between the magnetostatic interactions and intergranular exchange determines the number of spin-wave modes with finite k vectors that share the $k = 0$ (ferromagnetic resonance) frequency (the degeneracy), which is well known to affect the damping [2].

II. EXPERIMENTAL RESULTS

To determine the damping from the numerical model and experimentally we use an optical ferromagnetic resonance (FMR) method. In an optical FMR experiment, a magnetic field is used to force the magnetic moments away from their equilibrium. An optical pulse is applied, heating the sample, and thus leading to a new equilibrium position for the magnetization. The initial/new equilibrium configuration

*lja503@york.ac.uk
†thomas.ostler@ulg.ac.be

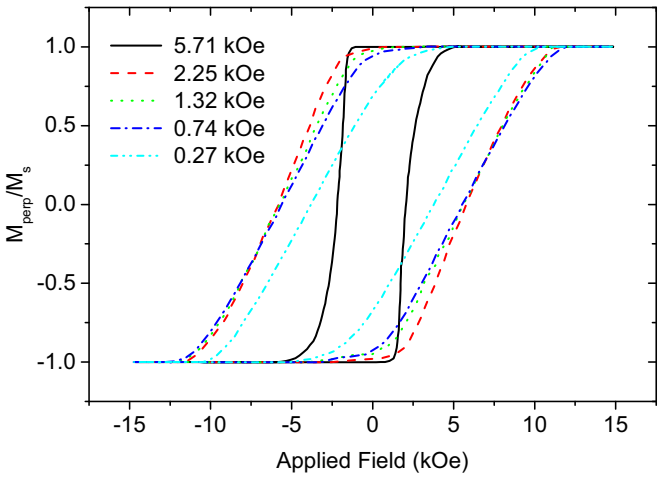

FIG. 1. Hysteresis loops for the series of CoPt with variable exchange. Increasing exchange leads to increasingly square loops as expected.

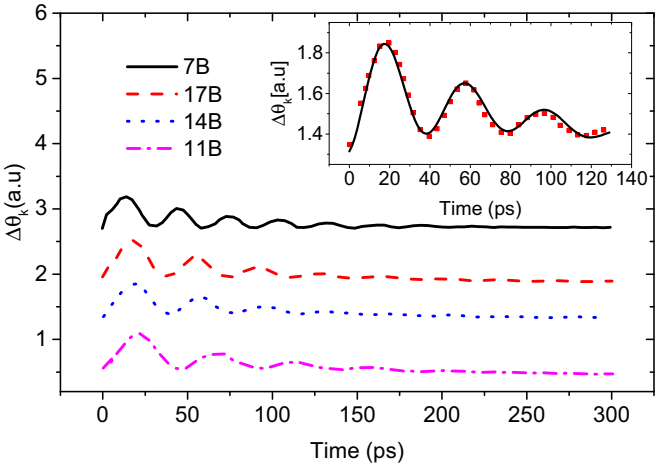

FIG. 2. Example of a time resolved magnetization trace determined experimentally. Also shown in the inset is an example of the fit to data that was used to extract the damping, where the raw data is shown as points and fitted function is shown as a line.

arises due to the minimization of the competing anisotropy, exchange, demagnetizing and Zeeman energies at the starting/final temperature. The rapid increase in temperature caused by the laser induces precession of those moments around a new position due to thermally induced changes in the energy contributions. The resulting dynamics can then be analyzed to determine effective parameters governing the relaxation process. This technique has been applied to a wide range of materials and structures [7–10]. In particular optical FMR is the preferred method for measuring the damping and resonance frequencies in materials with a strong magnetocrystalline anisotropy [11], due to the high fields required to drive the system to resonance in a typical ferromagnetic resonance experiment [12]. Interestingly, the two methods were shown to give the same values of the damping by Clinton and co-workers in Ref. [7].

We have carried out measurements on a series of CoPt perpendicular media in which the exchange coupling was varied by changing the oxygen content in the intergranular layers. The applied field is applied perpendicular to the sample plane (in the z direction). The variation of the exchange coupling is immediately apparent in the measured hysteresis loops as shown in Fig. 1, where it can be seen that increasing oxygen content gives rise to increasingly sheared loops as the intergranular exchange is reduced, due to the distribution of switching fields and the fact that the reduced exchange leads to a less coherent reversal mechanism.

From the hysteresis properties we determine the exchange field using $N * 4\pi M_s - H_{\text{int}}$, where N is a demagnetizing factor, usually anywhere between 0.75 and 0.85 [13], and H_{int} is the mean interaction field measured using FORC [14].

We have carried out measurements of the effective damping constant using the optically pumped FMR technique [15] in order to investigate the dependence of the effective damping constant on the exchange. The magnetic moments are forced away from the equilibrium position using a 0.8 kOe field at a 45° angle from the out of plane anisotropy axis. A 10.8 mW laser is used to heat the media and excite the magnetization into precession. An example of the time resolved magnetization data obtained is given in Fig. 2 which includes an example (inset) of the fit to the data that was used to determine the damping of the system.

The results are shown in Fig. 3, which shows the dependence of the measured Gilbert damping constant on the exchange field. The values of the damping are calculated by fitting the transverse magnetization components to a decaying oscillating function, $m_y(t) = A\ \cos(\omega t)\exp(-t/\tau)$, where the fitting parameters are A, the amplitude, ω, the resonance frequency, and τ, the relaxation rate. The damping is then $\alpha = 1/\tau\omega$.

A nonmonotonic dependence of α on H_{ex} is clear. In order to interpret the experiments in terms of the intergranular interactions we have also measured the zero field cluster size

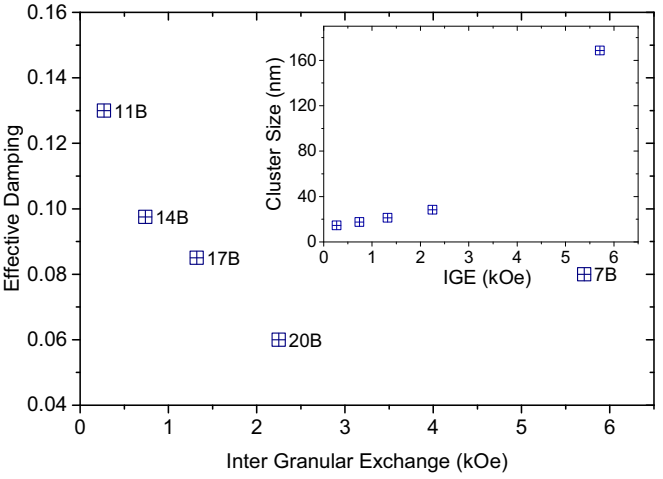

FIG. 3. Dependence of the measured Gilbert damping constant on the exchange field. A nonmonotonic dependence of α on H_{ex} is clear. (Inset) Variation of the cluster size with exchange field determined using the method given in Ref. [13] and described in the text.

using the method of Nemoto *et al.* [13]. The results are given in the inset of Fig. 3. Importantly, it is found that for the sample with the highest exchange coupling there is a large increase in the correlation length. This is consistent with the form of the hysteresis loop shown in Fig. 1, where the sample exhibits a very square loop consistent with magnetization by nucleation and propagation of quasidomains.

III. NUMERICAL MODEL

To corroborate the effects of increasing intergranular exchange we have constructed a dynamic numerical model of granular media using the Landau-Lifshitz-Bloch (LLB) equation [16] combined with a Voronoi construction of the grains typical for magnetic recording media. The interactions between the grains are calculated based on the interaction distances and lengths between the grains and included into the LLB model, both of which we describe in the following.

A. Landau-Lifshitz-Bloch model

The LLB equation of motion describes the time evolution of a magnetic macrospin. The equation allows for longitudinal relaxation of the magnetization, and was derived by Garanin [16] within a mean field approximation from the classical Fokker-Planck equation for atomic spins interacting with a heat bath. Models based on the resulting expressions have been shown to be consistent with atomistic spin dynamics simulations [17], as well as comparisons with experimental observations, for example, in laser induced demagnetization [18] and domain wall mobility measurements in yttrium iron garnet crystals close to the Curie point [19] (T_c). The equation is similar to the Landau-Lifshitz-Gilbert (LLG) equation [20], with precessional and relaxation terms, but with an extra term that deals with changes in the magnitude of the magnetization:

$$\dot{\mathbf{m}}_i = -\gamma\left[\mathbf{m}_i \times \mathbf{H}_i^{\text{eff}}\right] + \frac{\gamma\alpha_\parallel}{m_i^2}\left(\mathbf{m}_i \cdot \mathbf{H}_i^{\text{eff}}\right)\mathbf{m}_i - \frac{\gamma\alpha_\perp}{m_i^2}\left[\mathbf{m}_i \times \left[\mathbf{m}_i \times \mathbf{H}_i^{\text{eff}}\right]\right], \tag{1}$$

where $\mathbf{m}_i$ is a spin polarization. The spin polarization tends towards equilibrium, m_e, which is a temperature dependent input parameter (discussed below). $\alpha_\parallel$ and $\alpha_\perp$ are dimensionless longitudinal and transverse damping parameters. γ is the gyromagnetic ratio taken to be the free electron value. The LLB equation is valid for finite temperatures and even above T_c, though the damping parameters and effective fields are different below and above T_c. For the transverse damping parameter,

$$\alpha_\perp = \begin{cases} \lambda\left(1 - \frac{T}{3T_c}\right), & T < T_c, \\ \lambda\frac{2T}{3T_c}, & T \geqslant T_c, \end{cases} \tag{2}$$

and, for the longitudinal,

$$\alpha_\parallel = \lambda\frac{2T}{3T_c} \quad \text{for all } T. \tag{3}$$

For a single macrospin free energy density f is given by

$$f_i = -M_s(0)\mathbf{B}\cdot\mathbf{m}_i + \frac{M_s(0)}{2\tilde{\chi}_\perp}\left(m_{i,x}^2 + m_{i,y}^2\right) + \frac{M_s(0)}{8\tilde{\chi}_{i,\parallel}m_{i,e}^2}\left(m_i^2 - m_{i,e}^2\right)^2 - M_s(0)^2\sum_{j,i\neq j} V_i V_j \times \frac{3(\mathbf{m}_i\cdot\mathbf{e}_{ij})(\mathbf{m}_j\cdot\mathbf{e}_{ij}) - \mathbf{m}_i\cdot\mathbf{m}_j}{r_{ij}^3}, \tag{4}$$

and the effective fields, $\mathbf{H}_i^{\text{eff}} = -\frac{1}{M_s^0}\frac{\delta f}{\delta \mathbf{m}_i}$ are given by [16]:

$$\mathbf{H}_i^{\text{eff}} = \mathbf{B} + \mathbf{H}_{A,i} + \frac{1}{2\tilde{\chi}_{i,\parallel}}\left(1 - \frac{m_i^2}{m_{i,\text{e}}^2}\right)\mathbf{m}_i + \mathbf{H}_{\text{e,i}} + \mathbf{H}_{\text{dip,i}}, \tag{5}$$

where $\mathbf{B}$ represents an external magnetic field, $\mathbf{H}_{\text{dip,i}}$ is the dipolar field, and $\mathbf{H}_{A,i} = -(m_i^x\mathbf{e}_i^x + m_i^y\mathbf{e}_i^y)/\tilde{\chi}_\perp$ an anisotropy field. $M_s(0)$ is the saturation magnetization (magnetization at 0 K); V_i represents the volume of grain i. Here, the susceptibilities $\tilde{\chi}_l$ are defined by $\tilde{\chi}_l = \partial m_l/\partial H_l$. $\mathbf{H}_e$ is the (intergranular) exchange field, which we assume is based on the contact area between the grains, arising from the Voronoi construction, as discussed below. In these equations, λ is a microscopic parameter which characterizes the coupling of the individual, atomistic spins with the heat bath (the intrinsic damping). We choose the value of λ to be 0.05 for this work. It is worth pointing out that we expect the results and conclusions presented here to be qualitatively the same for all values of the damping. The calculation of the dipolar field is truncated at eight grain diameters to reduce the N^2 calculation over all pairwise interactions. The long-ranged contribution is then treated within a mean-field approximation.

For application of the LLB equation one has to know the spontaneous equilibrium magnetization $m_e(T)$, the perpendicular $[\tilde{\chi}_\perp(T)]$, and parallel $[\tilde{\chi}_\parallel(T)]$ susceptibilities beforehand. In this work, the input functions are based on that of Ref. [17] for FePt and scaled to give the correct Curie temperature. For the transverse susceptibility (that determines the anisotropy) the function is scaled to give an anisotropy constant of 13.5×10^6 erg/cc. The functions are scaled in the same manner as that of Ref. [21]:

$$M_s(T) = \frac{M_s(0)}{M_s^{\text{FePt}}(0)}M_s^{\text{FePt}}\left(\frac{T_C^{\text{FePt}}}{T_C}T\right), \tag{6}$$

$$\chi_\parallel(T) = \frac{M_s(0)}{M_s^{\text{FePt}}(0)}\chi_\parallel^{\text{FePt}}\left(\frac{T_C^{\text{FePt}}}{T_C}T\right), \tag{7}$$

$$\chi_\perp(T) = \frac{M_s(0)}{2K(0)}\chi_\perp^{\text{FePt}}\left(\frac{T_C^{\text{FePt}}}{T_C}T\right). \tag{8}$$

B. Granular model

The model of the magnetic nanostructures is based on a Voronoi construction which creates structures and grain size dispersions similar to those produced in magnetic hard disk drives (see Fig. 4). The seed points for the Voronoi algorithm are based on a 2D hexagonal structure with the points moved by a random value, linearly, to generate structural disorder.

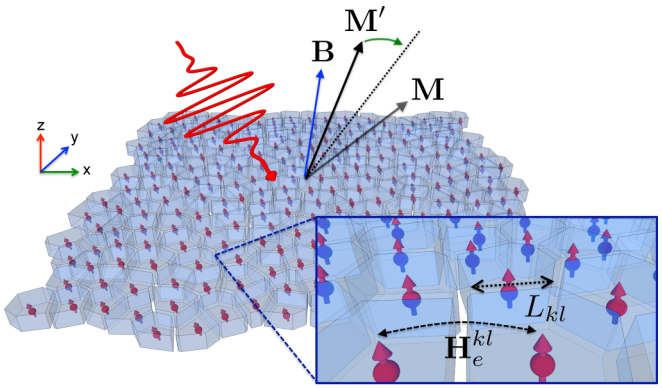

FIG. 4. Schematic of the setup of the simulations. The anisotropy is perpendicular to the plane with the applied field at an angle θ to the plane. The magnetization equilibrates to **M** before the laser pulse is applied. The laser pulse results in relaxation of the magnetization by precession to the new orientation, **M**′.

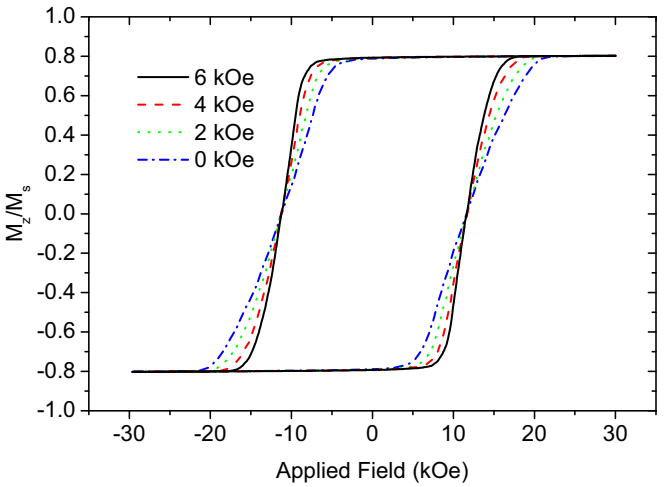

FIG. 5. Numerically calculated hysteresis curves for a range of intergranular exchange constants in good qualitative agreement with the experimental hysteresis loops (Fig. 1).

This results in a log-normal distribution of grain volumes, V_i, as seen experimentally. The average grain diameter in our numerical simulations is 8 nm with a thickness of 8 nm. The standard deviation in the grain diameter is 2.63 nm. In the present work we assume no dispersion in the anisotropy easy axes of the grains and we numerically simulate a system approximately 700 nm × 700 nm laterally, corresponding to 7558 grains. Furthermore, we do not assume a spatial variation of the anisotropy strength per grain, though the Voronoi construction gives a volume distribution giving rise to a variation of energy barrier, KV. This means that to first order the extrinsic contributions, from anisotropy, to the damping are zero [2].

The IGE is formulated on the basis of the contact area between grains as was implemented in Ref. [22]. Considering neighboring grains k and l, the exchange energy between them can be written

$$E_{\text{exch}}^{kl} = -N_{kl} J_{kl} \hat{\mathbf{s}}_k \cdot \hat{\mathbf{s}}_l, \tag{9}$$

where N_{kl} is the number of atoms in the contact area between (k,l). Assuming a film of uniform thickness t, $N_{kl} = L_{kl} t/a^2$, where L_{kl} is the contact length between the grains and a is the lattice constant. The exchange field on grain k due to l is therefore

$$\mathbf{H}_e^{kl} = -\frac{\partial E_{\text{exch}}^{kl}}{\partial \boldsymbol{\mu}_k} = \frac{L_{kl} J_{kl}}{a^2 M_s A_k} \hat{\mathbf{s}}_l. \tag{10}$$

A_k is the area of the face of grain k in the plane of thin film and L_{kl} is the contact length between grains k and l. In addition, we allow for some dispersion in the J_{kl} by generating a normal distribution with a given width. We now write Eq. (10) in terms of reduced parameters (relative to the median values L_m, A_m, J_m)

$$\mathbf{H}_e^{kl} = H_{\text{exch}} \left(\frac{J_{kl}}{J_m}\right)\left(\frac{L_{kl}}{L_m}\right)\left(\frac{A_m}{A_k}\right)\hat{\mathbf{s}}_l, \tag{11}$$

where $H_{\text{exch}} = J_m L_m/(a^2 M_s A_m)$. In practice H_{exch} is set by the requirement that the average exchange at saturation has a certain value $H_{\text{exch}}^{\text{sat}}$, which is the more accessible value experimentally, that is

$$H_{\text{exch}}^{\text{sat}} = N^{-1} H_{\text{exch}} \sum_k \sum_{l \in n.n} \left(\frac{J_{kl}}{J_m}\right)\left(\frac{L_{kl}}{L_m}\right)\left(\frac{A_m}{A_k}\right). \tag{12}$$

We have verified that the model gives consistent static results by initially simulating hysteresis loops for a range of intergranular exchange. Qualitatively Fig. 5 shows increasingly square loops with increasing intergranular exchange.

There are some expected quantitative differences between the experimental and numerically determined loops that primarily arise from the fact that the Landau-Lifshitz-Bloch equation is integrated numerically as a function of time; however, the total simulation time is orders of magnitude lower than those measured experimentally. Furthermore, the numerical simulations do not take into account the detailed variations in the experimental structure, saturation magnetization, anisotropy, or grain size variations. Not taking these specific aspects into account allows us to use the numerical model to interpret the experimental results without these extra degrees of freedom.

During the simulations of optically induced FMR we apply a magnetic field in the x-z plane at an angle θ which we take to be at 45° from the z axis of magnitude 10 kOe. The anisotropy is assumed to be uniaxial and points out of the plane of the sample. The large angle at which we apply the field gives rise to large amplitude precession giving excellent fits to the magnetization (discussed below). Even in the presence of the field at 45°, the large anisotropy ensures that the magnetization lies strongly out of plane. In our optical FMR approach we assume a square pulse in temperature rising from ambient to 600 K for 400 ps, returning to ambient after the pulse. In a real optical FMR experiment on the picosecond time scale the laser generates a hot electron distribution that can reach temperatures of thousands of kelvin [23]. Subsequently, the hot electrons reach a quasiequilibrium state with the phonons at the same temperature. Depending on the relaxation time of the magnetic system the spin system will reach equilibrium with this quasiequilibrium at around 0.1–1 ps [24], though this

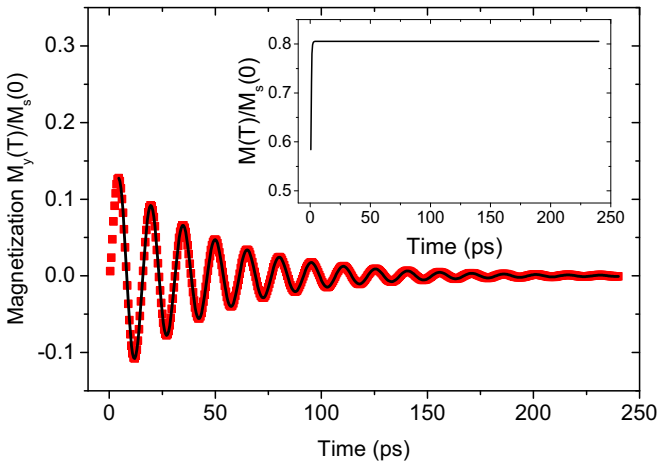

FIG. 6. Example of the transverse magnetization dynamics after a heat pulse (points) with a fit to the dynamics (lines). (Inset) Example of the longitudinal magnetization dynamics after a pulse.

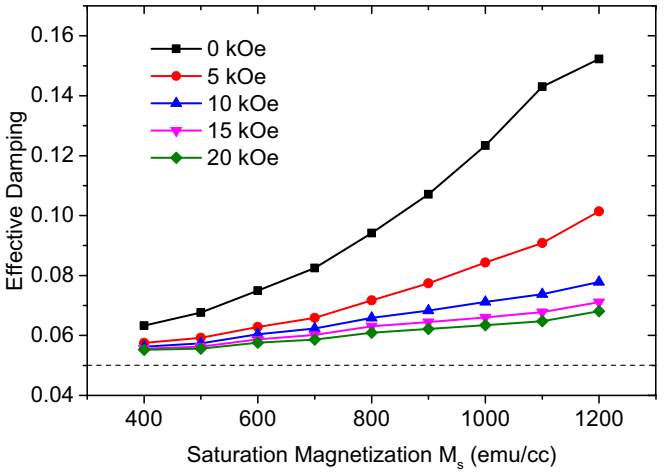

FIG. 7. Damping as a function of saturation magnetization for a range of values of the intergranular exchange, $H_{\text{exch}}^{\text{sat}}$.

can be considerably longer for pure rare earth metals [25]. For metallic ferromagnets, the changes in the magnitude of the magnetization occur on a much faster time scale than the resulting precession (see inset of Fig. 6); thus we probe the dynamics at the temperature after the pulse. Experimentally the long cooling time to the initial temperature occurs by transfer of energy out of the magnetic material to the substrate and the surroundings via phonon processes on the nanosecond time scale.

Using the LLB model, we have investigated the effects of varying the saturation magnetization and IGE on the damping of our granular material after excitation with a heat pulse. As discussed above, the change in temperature alters the equilibrium position, which causes the magnetization to precess back the initial state. An example of the resulting dynamics within the LLB model is shown in Fig. 6 (points). On the picosecond time scale the magnetization is quickly reduced, in agreement with experimental [26–28] and numerical results [28–30] so that the quenching and recovery of the anisotropy field is much faster than the time scale of the precessional dynamics.

Using the numerical model we first calculate the damping as a function of the saturation magnetization, as presented in Fig. 7, for a range of values of the IGE. The values for the damping are calculated as with the experimental data.

Figure 7 shows a strong variation and a subtle combination of contributions from magnetostatic and exchange interactions. Consider first the case $H_{\text{exch}}^{\text{sat}} = 0$. From Fig. 7 it can be seen that there is a very strong dependence of effective damping on M_s, specifically an increase of around a factor of 2.5 for M_s values around those of Co and Fe. For low values of M_s the damping for all values of IGE converge to the value of the input damping due to the very low contribution from the demagnetizing fields.

The variation of damping with IGE, determined numerically, is shown in Fig. 8 and is consistent with the experimentally observed decrease (Fig. 3) in damping with increasing intergranular exchange. For low values of the saturation magnetization the value of the damping shows very little variation and remains close to the value for the intrinsic damping used for the calculations. For larger values of M_s there is a much larger variation with IGE where there is a strong interplay between the demagnetizing energy and the IGE.

Overall, the numerical simulations are consistent with the experimental data for small exchange fields, where the effective damping is seen to decrease with H_{ex}. However, the model does not reproduce the increase in damping for the sample with the largest exchange (see Fig. 3). This is likely related to the dramatic increase in the measured cluster size for this particular sample as shown in the inset of Fig. 3. For this sample, the oxide concentration was reduced to zero, and it is possible that the determined exchange field is an underestimate. The large cluster size and the form of the hysteresis loop for this sample is indicative of a change to a nucleation/propagation mechanism, which is not observed in

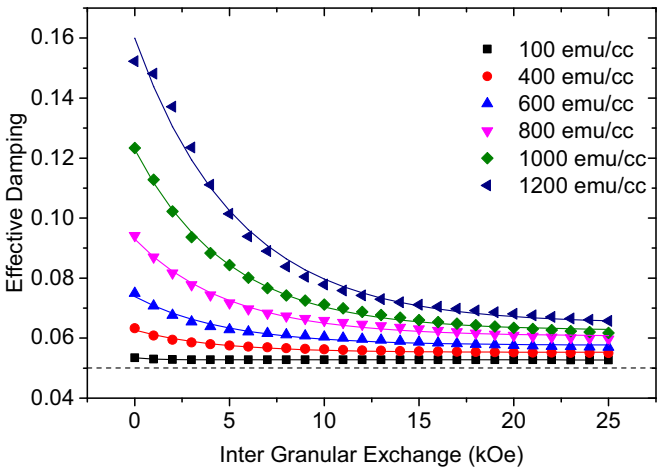

FIG. 8. Damping as a function of intergranular exchange for a range of values of saturation magnetization. For low values of M_s the value of the damping varies very little and remains around the value of the input damping parameter. As M_s increases, the variation with intergranular exchange becomes much greater as the interplay between the demagnetizing fields and exchange becomes important.

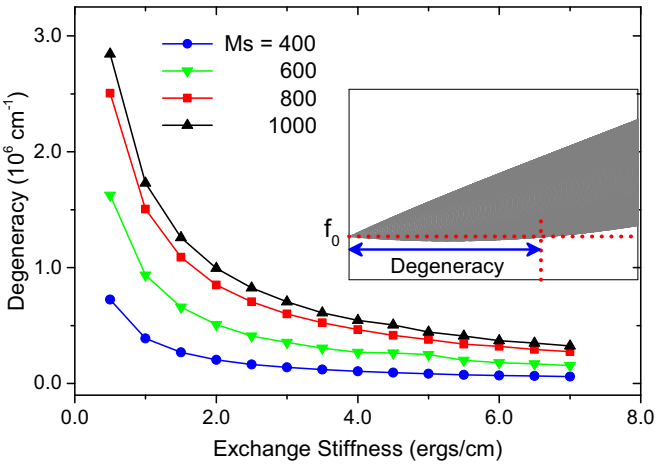

FIG. 9. Spin-wave degeneracy (shown schematically in the inset) as a function of exchange stiffness for a range of values of saturation magnetization. There is clearly a direct correlation between the degeneracy and the damping shown in Fig. 3 and a similar trend for fixed exchange stiffness and varying M_s.

the model calculations for values of H_{ex} up to 5 kOe. For a very strongly exchange coupled sample it is likely that additional damping mechanisms will arise from interaction of the domain walls with defects and impurities resulting in the increase in Gilbert damping at large exchange fields.

IV. SEMIANALYTICAL SPIN-WAVE MODEL

So far we have presented numerical and experimental results that show good agreement on the effects of interactions on the damping in granular media; however, the underlying mechanism remains somewhat ambiguous. In the following we ascribe the reduction in damping due to increasing intergranular exchange as arising from a reduction in the degeneracy of finite k vectors with the frequency of the $k = 0$ (ferromagnetic resonance) mode (see schematic inset of Fig. 9). In general, the presence of defects, inhomogeneities, boundaries, etc. can act as scattering centers leading to the energy transfer from the uniform magnetization precession into degenerate spin-wave modes. A reduction in this degeneracy reduces the number of possible spin-wave modes that can be scattered to or from. The process involves the annihilation of a zero-wave-number magnon and the creation of a nonzero-wave-number magnon. The consequence of this process is that the magnetization precession undergoes rapid relaxation (damping) [31]. Reducing this degeneracy will then result in a reduced damping. We conclude that the reduction of two-magnon scattering processes is dominating the reduction in damping due to increased intergranular exchange. To elucidate this we follow the method of McMichael [2,3,32]. In the present work we only briefly outline the method of determining the frequencies of the spin-wave modes. In Refs. [2,3,32] the Landau-Lifshitz-Gilbert equation is linearized. The resulting linearized components of the magnetization and fields are written in Fourier space through

$$b(\mathbf{r}) = \int \frac{d\mathbf{k}}{(2\pi)^2} b(\mathbf{k}) \exp(i\mathbf{k}\cdot\mathbf{r}), \tag{13}$$

where b represents the magnetization or the fields. The effective field has contributions from the Zeeman, demagnetizing, anisotropy, and exchange terms and is written in terms of a sum over the magnetization multiplied with a kernel, G, and is translationally invariant. Due to the $\mathbf{r} - \mathbf{r}'$ term, on-site terms would be represented by delta functions multiplied by a scalar. The Fourier components of the field are then written:

$$\mathbf{H}_{\text{eff}}(\mathbf{r}) = \int d\mathbf{r}' G(\mathbf{r} - \mathbf{r}')\mathbf{m}(\mathbf{r}'), \tag{14}$$

The Fourier component of this field are then, $\mathbf{H}(\mathbf{k}) = -\mathbf{h}_\mathbf{k}\mathbf{m}(\mathbf{k})$, where $\mathbf{h}_\mathbf{k}$ are the elements of the normalized stiffness tensor:

$$h_{\theta\theta,\mathbf{k}} = M_s^{0-1}[H_i + Dk^2 + M_s^0(1 - N_k)\sin^2(\theta_k)], \tag{15a}$$

$$h_{\phi\phi,\mathbf{k}} = M_s^{0-1}[H_i + Dk^2 + M_s^0 N_k \cos^2(\phi)] + M_s^0(1 - N_k)\sin^2(\phi)\cos^2(\theta_k), \tag{15b}$$

$$h_{\theta\phi,\mathbf{k}} = M_s^{0-1}\big[M_s^0(1 - N_k)\cos(\theta_k)\sin(\theta_k)\sin(\phi)\big], \tag{15c}$$

$$h_{\phi\theta,\mathbf{k}} = h_{\theta\phi,\mathbf{k}}, \tag{15d}$$

where $Dk^2 = (2A/\mu_0 \mathrm{M}_s)k^2$ is the exchange field for a spin wave with wave vector $\mathbf{k}$, assuming that the wavelengths of interest are much larger than the lattice spacing. A is the exchange stiffness and $H_i = B\cos(\phi - \phi_H) - (M_s^0 - H_k)\sin^2(\phi)$ is the "internal field" consisting of the component of the following: the applied field B (at an angle ϕ_H to the plane) parallel to the magnetization, which is at an angle, ϕ, to the plane, the static part of the demagnetization field, and the anisotropy field H_k. The k-dependent demagnetization factor for a film of thickness d is given by

$$N_k = \frac{1 - e^{-kd}}{kd}. \tag{16}$$

The susceptibility tensor, $\chi_\mathbf{k}(\omega)$, can be obtained from the linearized LLG equations of motion. For an applied field with spatial frequency $\mathbf{k}$ and angular frequency ω, the transverse susceptibility tensor is given by

$$\chi_\mathbf{k}(\omega) = \frac{1}{Z_\mathbf{k}}\begin{bmatrix} h_{\phi\phi,\mathbf{k}} + \frac{i\alpha\omega}{\omega_M} & -h_{\theta\phi,\mathbf{k}} + \frac{i\alpha\omega}{\omega_M} \\ -h_{\phi\theta,\mathbf{k}} - \frac{i\alpha\omega}{\omega_M} & h_{\theta\theta,\mathbf{k}} + \frac{i\alpha\omega}{\omega_M} \end{bmatrix}, \tag{17a}$$

$$Z_\mathbf{k} = h_{\theta\theta,\mathbf{k}}h_{\phi\phi,\mathbf{k}} - h_{\theta\phi,\mathbf{k}}h_{\phi\theta,\mathbf{k}} - (1 + \alpha^2)\Big(\frac{\omega}{\omega_M}\Big)^2 + i\alpha\Big(\frac{\omega}{\omega_M}\Big)(h_{\theta\theta,\mathbf{k}} + h_{\phi\phi,\mathbf{k}}), \tag{17b}$$

where $\omega_M = \gamma M_s^0$. The dispersion relation is obtained by noting that $|Z_\mathbf{k}|$ is minimum and the susceptibility is in resonance when

$$\omega = \omega_\mathbf{k} = \frac{\omega_M}{\sqrt{1 + \alpha^2}}[h_{\theta\theta,\mathbf{k}}h_{\phi\phi,\mathbf{k}} - h_{\theta\phi,\mathbf{k}}h_{\phi\theta,\mathbf{k}}]^{1/2}. \tag{18}$$

To make a consistent comparison between the LLB numerical model and the spin-wave model we use the values of M_s, anisotropy, thickness (d), applied field, and applied field angle that are the same in both cases. Furthermore, the angles of the magnetization (ϕ) from the film plane are taken directly from the numerical simulations at equilibrium after

the pulse (from the end of the numerical simulation). Using the physical parameters that enter into the LLB model we have calculated the spin-wave properties of the numerically simulated samples using Eqs. (15)–(18) and determined the degeneracy of those modes with the $k = 0$ mode. This plays an important role in the damping arising from inhomogeneities [2] due to nonuniformities that are present in granular media. We note that the value of the exchange stiffness that enters into the equations is in the correct range [4] for granular media but it is not trivial to relate the intergranular exchange field in the LLB with the long-wavelength exchange, A, used in the spin-wave model. We note here that the presented form of the semianalytical spin-wave model does not take into account inhomogeneous line broadening effects, and thus contains contributions only from inhomogeneities which arise in the LLB model from the distribution of the grain volumes. The results of the semianalytical spin-wave model are shown in Fig. 9 and show a decreasing trend with increasing exchange stiffness.

We can conclude that the two-magnon scattering process is the leading term in our reduction in damping with intergranular exchange and is strongly affected by the interactions due to intergranular exchange and the demagnetizing fields. This is supported by the fact that the LLB model does not include any specific detail about the grain boundaries or dispersions in the anisotropy axes or on-site magnitudes, though does take into account different demagnetizing fields, size distribution, etc., so there is inevitably a distribution in the cone angle of the macrospins. Therefore, scattering with impurities cannot occur. The role of grain-to-grain scattering due to slight dispersions in the anisotropy axes is zero in our LLB model as we assume perfectly aligned anisotropy axes. Similarly, we assume that our grains are uniform single macrospins and therefore grain-boundary scattering cannot contribute to this two-magnon scattering process. In terms of a macrospin picture, the decreased damping can be explained by a stiffening of the system resulting in a more coherent precession so that demagnetizing effects become less important and the system as a whole acts more like a single macrospin.

V. CONCLUSION

In summary we have carried out an investigation of the effects of intergranular interactions on the effective damping constant of perpendicular media. Experiments show a nonmonotonic variation of the damping with increasing exchange strength. Contributions to the experimental damping constant due to inhomogeneous line broadening cannot be ruled out, however, these are expected to be consistent between samples; the major effect of reducing the thickness of the grain boundaries is the variation in the exchange coupling as shown in the hysteresis behavior. We have constructed a realistic model of granular media using the Landau-Lifshitz-Bloch model. By simulating the optical FMR technique to probe relaxation processes we have determined how the damping is affected by the key parameters governing the interactions (exchange and saturation magnetization). The model calculations show a decrease of effective damping with increasing exchange, consistent with the experimental data for small exchange. It is argued that the increase in damping for the largest exchange field, arising in a film without exchange coupling, is due to the onset of a different reversal mechanisms involving domain nucleation and propagation. For practical perpendicular recording media, which are more exchange decoupled, the decrease in damping with exchange strength predicted by the model calculations is the most likely scenario. Further investigations of the phenomenon using spin-wave theory provide further insight and ascribe the reduction in damping due to increasing intergranular exchange as arising from a reduction in the degeneracy of finite k vectors with the frequency of the $k = 0$ (ferromagnetic resonance) mode. These calculations show a direct correlation between the degeneracy and the damping shown by the numerical model with a similar trend for fixed exchange stiffness and varying M_s. Our numerical calculations do not include extrinsic contributions to damping due to variations in on-site quantities, such as anisotropy or saturation magnetization; thus we have shown that it is possible to describe the decrease in damping with intergranular exchange based on the effects of intergranular exchange and demagnetizing fields; thus we conclude that their contribution is large.

ACKNOWLEDGMENTS

This work was supported by the European Commission under Contract No. 281043, *Femtospin*. The financial support of the Advanced Storage Technology Consortium is gratefully acknowledged. T.A.O. gratefully acknowledges the support of the Marie Curie incoming BeIPD-COFUND fellowship program at the University of Liège.

The authors L.J.A. and T.A.O. contributed equally to this work.

[1] V. Sokalski, D. E. Laughlin, and J.-G. Zhu, Appl. Phys. Lett. **95**, 102507 (2009).
[2] R. D. McMichael, J. Appl. Phys. **95**, 7001 (2004).
[3] R. McMichael and P. Krivosik, IEEE Trans. Magn. **40**, 2 (2004).
[4] P. Krone, M. Albrecht, and T. Schrefl, J. Magn. Magn. Mater. **323**, 432 (2011).
[5] A. Butera, Eur. Phys. J. B **52**, 297 (2006).
[6] N. Mo, J. Hohlfeld, M. ul Islam, C. S. Brown, E. Girt, P. Krivosik, W. Tong, A. Rebei, and C. E. Patton, Appl. Phys. Lett. **92**, 022506 (2008).
[7] T. W. Clinton, N. Benatmane, J. Hohlfeld, and E. Girt, J. Appl. Phys. **103**, 07F546 (2008).
[8] S. S. Kalarickal, N. Mo, P. Krivosik, and C. E. Patton, Phys. Rev. B **79**, 094427 (2009).
[9] A. Mekonnen, M. Cormier, A. V. Kimel, A. Kirilyuk, A. Hrabec, L. Ranno, and T. Rasing, Phys. Rev. Lett. **107**, 117202 (2011).
[10] X. Zou, J. Wu, P. K. J. Wong, Y. B. Xu, R. Zhang, Y. Zhai, C. Bunce, and R. W. Chantrell, J. Appl. Phys. **109**, 07D341 (2011).

[11] J. Becker, O. Mosendz, D. Weller, A. Kirilyuk, J. C. Maan, P. C. M. Christianen, T. Rasing, and A. Kimel, Appl. Phys. Lett. **104**, 152412 (2014).
[12] T. A. Ostler, M. O. A. Ellis, D. Hinzke, and U. Nowak, Phys. Rev. B **90**, 094402 (2014).
[13] H. Nemoto, I. Takekuma, H. Nakagawa, T. Ichihara, R. Araki, and Y. Hosoe, J. Magn. Magn. Mater. **320**, 3144 (2008).
[14] C. R. Pike, A. P. Roberts, and K. L. Verosub, J. Appl. Phys. **85**, 6660 (1999).
[15] M. van Kampen, C. Jozsa, J. T. Kohlhepp, P. LeClair, L. Lagae, W. J. M. de Jonge, and B. Koopmans, Phys. Rev. Lett. **88**, 227201 (2002).
[16] D. A. Garanin, Phys. Rev. B **55**, 3050 (1997).
[17] N. Kazantseva, D. Hinzke, U. Nowak, R. W. Chantrell, U. Atxitia, and O. Chubykalo-Fesenko, Phys. Rev. B **77**, 184428 (2008).
[18] J. Mendil, P. Nieves, O. Chubykalo-Fesenko, J. Walowski, T. Santos, S. Pisana, and M. Münzenberg, Sci. Rep. **4**, 3980 (2014).
[19] J. Kötzler, D. A. Garanin, M. Hartl, and L. Jahn, Phys. Rev. Lett. **71**, 177 (1993).
[20] T. Gilbert, IEEE Trans. Magn. **40**, 3443 (2004).
[21] K. M. Lebecki and U. Nowak, J. Appl. Phys. **113**, 023906 (2013).
[22] Y. Peng, X. W. Wu, J. Pressesky, G. P. Ju, W. Scholz, and R. W. Chantrell, J. Appl. Phys. **109**, 123907 (2011).
[23] J. Chen, D. Tzou, and J. Beraun, Int. J. Heat Mass Transfer **49**, 307 (2006).
[24] I. Radu, C. Stamm, A. Eschenlohr, F. Radu, R. Abrudan, K. Vahaplar, T. Kachel, N. Pontius, R. Mitzner, K. Holldack, A. Föhlisch, T. A. Ostler, J. Mentink, R. Evans, R. W. Chantrell, A. Tsukamoto, A. Itoh, A. Kirilyuk, A. Kimel, and T. Rasing, SPIN **05**, 1550004 (2015).
[25] B. Koopmans, G. Malinowski, F. Dalla Longa, D. Steiauf, M. Fähnle, T. Roth, M. Cinchetti, and M. Aeschlimann, Nat. Mater. **9**, 259 (2010).
[26] E. Beaurepaire, J.-C. Merle, A. Daunois, and J.-Y. Bigot, Phys. Rev. Lett. **76**, 4250 (1996).
[27] I. Radu, K. Vahaplar, C. Stamm, T. Kachel, N. Pontius, H. A. Dürr, T. A. Ostler, J. Barker, R. F. L. Evans, R. W. Chantrell, A. Tsukamoto, A. Itoh, A. Kirilyuk, T. Rasing, A. V. Kimel, and H. a. Dürr, Nature (London) **472**, 205 (2011).
[28] K. Vahaplar, A. M. Kalashnikova, A. V. Kimel, D. Hinzke, U. Nowak, R. Chantrell, A. Tsukamoto, A. Itoh, A. Kirilyuk, and T. Rasing, Phys. Rev. Lett. **103**, 117201 (2009).
[29] T. A. Ostler, J. Barker, R. F. L. Evans, R. W. Chantrell, U. Atxitia, O. Chubykalo-Fesenko, S. El Moussaoui, L. Le Guyader, E. Mengotti, L. J. Heyderman, F. Nolting, A. Tsukamoto, A. Itoh, D. Afanasiev, B. A. Ivanov, A. M. Kalashnikova, K. Vahaplar, J. Mentink, A. Kirilyuk, T. Rasing, and A. V. Kimel, Nat. Commun. **3**, 666 (2012).
[30] U. Atxitia, J. Barker, R. W. Chantrell, and O. Chubykalo-Fesenko, Phys. Rev. B **89**, 224421 (2014).
[31] L. Lu, Z. Wang, G. Mead, C. Kaiser, Q. Leng, and M. Wu, Appl. Phys. Lett. **105**, 012405 (2014).
[32] R. D. McMichael, D. J. Twisselmann, and A. Kunz, Phys. Rev. Lett. **90**, 227601 (2003).